Collapse of magnetic moment drives the Mott transition in MnO

JAN KUNEŠ[1,2]*, ALEXEY V. LUKOYANOV[3], VLADIMIR I. ANISIMOV[4], RICHARD T. SCALETTAR[5] AND WARREN E. PICKETT[5]

[1]Theoretical Physics III, Center for Electronic Correlations and Magnetism, Institute of Physics, University of Augsburg, Augsburg 86135, Germany
[2]Institute of Physics, Academy of Sciences of the Czech Republic, Cukrovarnická 10, 162 53 Praha 6, Czech Republic
[3]Ural State Technical University-UPI, 620002 Yekaterinburg, Russia
[4]Institute of Metal Physics, Russian Academy of Sciences-Ural Division, 620041 Yekaterinburg GSP-170, Russia
[5]Department of Physics, University of California Davis, Davis, California 95616, USA
*e-mail: jan.kunes@physik.uni-augsburg.de

Published online: 3 February 2008; doi:10.1038/nmat2115

The metal–insulator transition in correlated electron systems, where electron states transform from itinerant to localized, has been one of the central themes of condensed-matter physics for more than half a century. The persistence of this question has been a consequence both of the intricacy of the fundamental issues and the growing recognition of the complexities that arise in real materials, when strong repulsive interactions play the primary role. The initial concept of Mott was based on the relative importance of kinetic hopping (measured by the bandwidth) and onsite repulsion of electrons. Real materials, however, have many further degrees of freedom that, as is recently attracting note, give rise to a rich variety of scenarios for a 'Mott transition'. Here, we report results for the classic correlated insulator MnO that reproduce a simultaneous moment collapse, volume collapse and metallization transition near the observed pressure, and identify the mechanism as collapse of the magnetic moment due to an increase of crystal-field splitting, rather than to variation in the bandwidth.

We consider, as one of the simpler examples of the canonical Mott insulators[1,2], the rock-salt-structure transition-metal monoxide (TMMO) manganese oxide with a half-filled $3d$ shell. MnO is, most certainly, a multi-orbital multi-electron system with the accompanying complexities of the tenfold degeneracy, but the half-filled $3d$ states under ambient conditions lead to a spherical spin-only magnetic moment. Applying pressure to such a system leads to a number of changes, including insulator–metal transition, orbital repopulation, moment reduction and volume collapse if a first-order transition results. These changes may occur simultaneously, or sequentially over a range of volumes[3]. Any of these may be accompanied by a structural phase transition, that is, a change in crystal symmetry, but an isostructural volume collapse may occur as well. The $3d$ bandwidth of such a Mott insulator is very susceptible to applied pressure, and has been thought to be one of the main controlling factors in the transition.

Although MnO's half-filled shell seems to give it a connection to well-studied models, this aspect also makes it atypical of transition-metal monoxides, as shown by Saitoh *et al.* who compiled[4] effective parameters for TMMOs from spectroscopic information. An effective intra-atomic Coulomb repulsion energy U_{eff} as defined by them is roughly twice as large as for the other $3d$ monoxides, and this has been used to suggest that MnO may be the most strongly correlated TMMO. The complexity that should be expected can be grasped by listing the relevant energy scales: $3d$ bandwidth W, Coulomb repulsion U, intra-atomic d–d exchange energy (Hund's rule) J, crystal-field splitting $\Delta_{\mathrm{cf}} = \varepsilon_{e_g} - \varepsilon_{t_{2g}}$ and charge transfer energy $\Delta_{\mathrm{ct}} \equiv \varepsilon_{t_{2g}} - \varepsilon_p$ (the difference in Mn $3d$ (we use t_{2g}) and O $2p$ site energies). All of these scales evolve as the volume decreases, altering the various microscopic processes and making the pressure-driven Mott transition a challenging phenomenon to describe.

Early shock data[5], and then Raman and optical studies[6,7], had identified a transformation in MnO at around 90–105 GPa. Transport[8], magnetic[8], structural and spectroscopic[9,10], and reflectivity[6] data all point to a first-order, insulator–metal Mott transition near 100 GPa with (reduced) volume ($v = V/V_\circ$) collapse $v = 0.68 \rightarrow 0.63$ and moment collapse (from $\sim 5\,\mu_B$ to $1\,\mu_B$ or less[9,10]). The structural data indicate a B1 $\rightarrow$ B8 change just before the Mott transition, which thus occurs within the B8 (NiAs) phase rather than the B1 (NaCl) phase. As the local environment of the Mn ion remains the same, this structural change is not expected to have much effect on the Mott transition in the disordered phase. Further discussion of experimental studies of the Mott transition in MnO is given in the Supplementary Information.

Dynamical mean field theory[11–13] (DMFT) as an approach for studying real materials has been showing impressive successes[14–22]. The method that we have implemented and applied (see the Methods section) moves the treatment significantly beyond the methods used earlier for TMMOs, by including a full thermodynamic average of local dynamic processes resulting from the strong interaction and all orbitals that can be relevant. Cohen *et al.* calculated the energy and magnetic moment using only local-density-approximation (LDA)-based interactions[23]. In LDA, MnO metallizes at (much too) low pressure; within the metallic phase, they obtained a moment and volume collapse around 150 GPa. Fang and collaborators addressed this difficulty by using LDA only for the high-pressure phase, and modelling

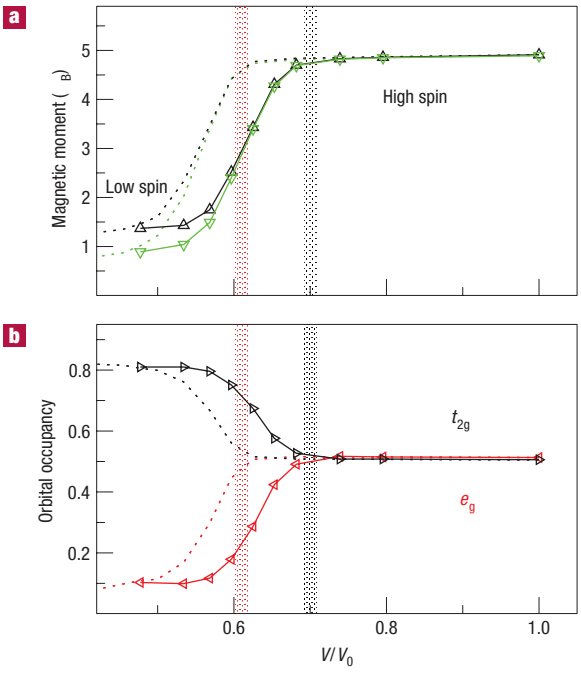

Figure 1 Evolution of the local magnetic moment and Mn 3*d* occupancies with volume. The decrease in the local moment correlates with the orbital occupations. **a**,**b**, Average instantaneous local moment M_s (black) and effective local moment M_{eff} (green) (**a**), and comparison to the Mn 3*d* orbital occupancies (**b**) resolved into e_g (red) and t_{2g} (black) components. The solid lines represent the results obtained with the physical values $U = 6.9$ eV, $J = 0.86$ eV; the dashed lines using the enhanced value $J = 1$ eV and constant U/J ratio illustrate how the moment collapse is suppressed to a smaller volume if the spin-exchange coupling is increased. Closing of the t_{2g} and e_g gaps is indicated by the black and red vertical lines respectively, confirming a connection between metallization and moment collapse. The analogous closing of the gaps for the dotted line case ($J = 1$ eV) is shifted correspondingly (not shown here).

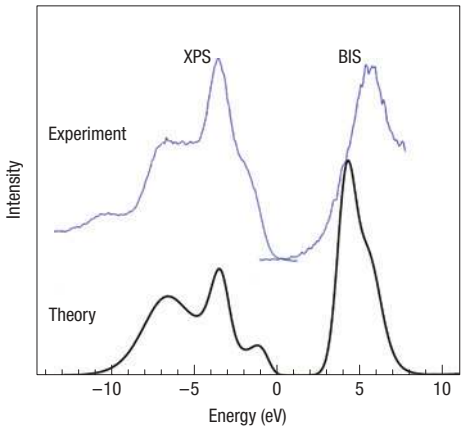

Figure 2 Ambient-pressure X-ray photoemission spectroscopy and bremsstrahlung isochromat spectroscopy data of van Elp *et al.*[29] on both sides of the energy gap for MnO. XPS: X-ray photoemission spectroscopy; BIS: bremsstrahlung isochromat spectroscopy. The upper curve, offset for clarity, is to be compared with the present DMFT result (bottom curve). Although the separation of the main peaks is underestimated by ~10%, the overall agreement in positions of structure is excellent.

the low-pressure phase with the correlated LDA + U method[24]. With two different functionals, however, it is not possible to obtain the transition pressure. Four correlated electronic structure methods[25], applied throughout the volume range of interest, have probed the behaviour of MnO under pressure; all obtained a high-spin ($S = 5/2$) to low-spin ($S = 1/2$) moment collapse but their predictions differed considerably in other respects, demonstrating that the dynamic treatment of correlation effects is crucial. The prediction of the LDA + U method, which is regarded as the static, $T = 0$ limit of the LDA + DMFT theory used here, is found to be affected by magnetic order[26], and predicts a zero-temperature moment collapse in an insulator–insulator transition around 120 GPa (the pressure depends on the value of J), with little difference between the B1 and B8 structure results. Thermodynamic fluctuations have not been included in any previous study of MnO.

MAGNETIC-MOMENT COLLAPSE AND METALLIZATION

Following most closely the approach developed and implemented by McMahan and co-workers[15,27,28] for pressure studies of elemental lanthanides, we have addressed the pressure-driven collapse of the correlated insulating state, using MnO as the prototype. Figure 1 shows the evolution of the local magnetic moment and Mn 3*d* occupancies with volume. We use two different measures of the local moment: (1) the mean instantaneous moment defined as an equal-time correlation function $M_s = \sqrt{\langle \hat{m}_z^2 \rangle}$ and (2) effective local moment defined through the local spin susceptibility $M_{eff} = \sqrt{T\chi_{loc}}$. These two moments have similar T-independent values in materials with Curie–Weiss behaviour. Under compression, the local moment and Mn 3*d* orbital occupancies retain their ambient-pressure high-spin values ($S = 5/2$) down to about $v = 0.68$. Further compression rapidly degrades the moment, which is accompanied by redistribution of electrons $e_g \rightarrow t_{2g}$ within the Mn 3*d* shell. The local moments and orbital occupancies start to level off to the low-spin values around $v = 0.57$. The reduction of M_{eff} below M_s in the low-spin state indicates that the local moment screening (charge fluctuations) is enhanced in comparison with the high-spin state.

Next we address the spectral properties, where the shortcomings of the LDA spectrum have been clear for decades. Figure 2 shows a comparison of the calculated total Mn 3*d* spectral function at ambient pressure with the photoemission data of van Elp *et al.*[29]. Excellent agreement is obtained for the gap and for the peak positions. (We note that using the enhanced value of $J = 1$ eV gives significantly poorer agreement.) Having obtained a correct ambient-pressure spectrum, we proceed in the study of the Mott transition by following the evolution with decreasing volume of the symmetry-resolved (t_{2g}, e_g) spectral densities, shown in Fig. 3. The onset of the moment collapse around $v = 0.68$ is signalled by, and associated with, closing of the gap in the t_{2g} channel, whereas the e_g gap is still visible at $v = 0.63$. This orbital selectivity[30,31] in metallization cannot be an exact property because both e_g and t_{2g} bands hybridize with the same O 2*p* bands throughout the Brillouin zone; however, the smallness of t_{2g}–2*p* mixing allows the orbital selectivity to be remarkably pronounced. As the t_{2g} gap closes, a quasiparticle peak appears at the chemical potential ($E = 0$) as has been seen in simple models[12]. Once in the low-spin state, the spectral functions bear strong resemblance to the parent LDA bands. In particular, the LDA ($U = J = 0$) t_{2g} spectrum contains a sharp peak just at/below the chemical potential, so it is not certain how much of the peak arising at the transition is due to the many-body nature of the system.

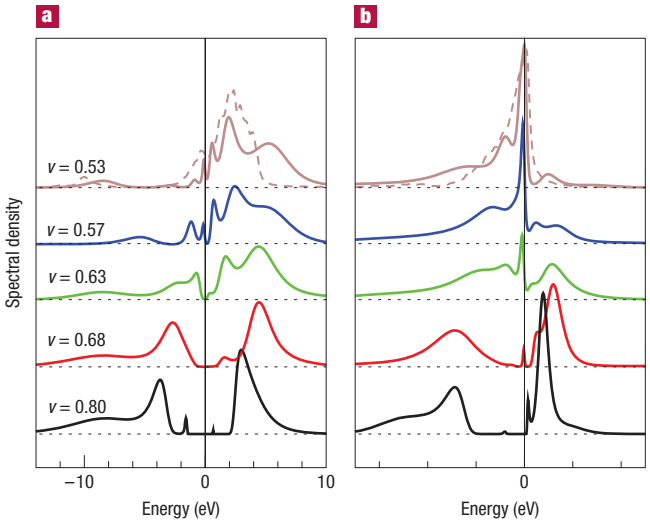

Figure 3 View of the evolution of the Mn 3*d* spectral densities under pressure. (Pressure increasing from bottom to top.) **a**,**b**, The single-particle spectral functions are resolved into e_g (**a**) and t_{2g} (**b**) irreducible representations for varying relative volume. Note the spectral weight shift under pressure: de-occupation of e_g occurs as the increase in occupation of t_{2g} proceeds (occupation ≡ integrated weight over negative energies). For the lowest volume, we show the uncorrelated (LDA) spectra for comparison (dashed lines). Apparently the main spectral features at high pressure originate from the uncorrelated band structure with some many-body renormalization. At even higher pressures, the spectra remain qualitatively unchanged with some reduction of the weight of the high-energy shoulders.

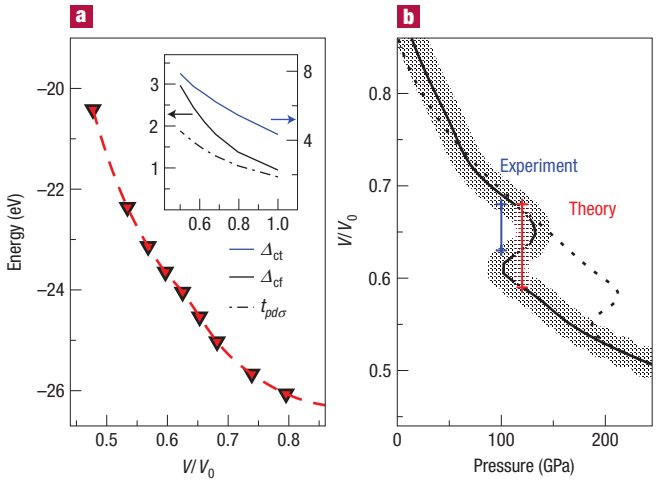

Figure 5 Two representations of the equation of state that quantifies the volume collapse transition. a,**b**, The internal energy versus volume (dashed line represents a spline interpolation) (**a**) and the resulting volume versus pressure curve (shading indicates estimated uncertainty) (**b**), obtained as a derivative of the spline interpolation of $E(V)$. The red bar on the $V(P)$ curve lying at the theoretical transition pressure $P_c^{th} = 120 \pm 15$ GPa determines the volume collapse $v = 0.68 \rightarrow 0.59$. The dotted curve represents $V(P)$ for the enhanced value of exchange $J = 1$ eV, showing the shift of the Mott transition to higher pressure with larger J. The width of the shaded red bar indicates the uncertainty of P_c^{th} due to the stochastic nature of the QMC method. The inset in **a** shows the evolution of selected tight-binding parameters (units of electronvolts); note the factor of three increase in Δ_{cf}.

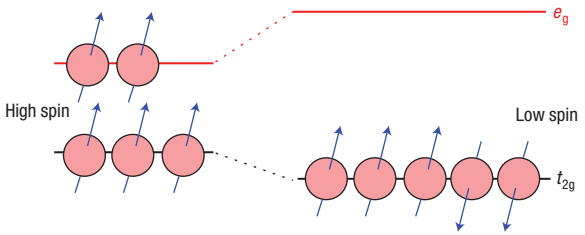

Figure 4 Schematic energy diagrams of the spin states at both ambient pressure and at high pressure in the collapsed phase. Occupations of the Mn 3*d* levels are shown for both high spin (left) and low spin (right). In the high-spin state, two spin-up electrons occupy e_g orbitals at the cost of $2\Delta_{cf}$ in energy, but the spin-exchange energy gain is $-10J$ ($5 \times 4/2 = 10$ pairs of parallel spin electrons). In the low-spin state, the crystal-field energy cost has become too great, and although the spin-exchange energy is less ($-4J$ from $3 \times 2/2$ (up) $+ 1$ (down) $= 4$ pairs) there is a net energy gain. The LDA energy difference is also a factor.

MECHANISM OF THE MOTT TRANSITION IN MnO

We now address a fundamental point of this work, namely the connection between moment collapse and metal–insulator transition, by observation of the impact of pressure on the effective hamiltonian. As U and J do not change, the pressure enters the calculation only through the quadratic (one-electron) part of the effective hamiltonian. Reducing the role of pressure down to fundamentals, we end up with two effects: (1) broadening of the 3*d* bands and (2) increase of the crystal-field splitting Δ_{cf}, which is shown schematically in Fig. 4 along with the state occupations. (We define Δ_{cf} in terms of the site energies of the e_g and t_{2g} Wannier functions; the e_g–t_{2g} band splitting is substantially larger owing to ligand field effects.) The evolution of the leading band structure quantities, which are the nearest-neighbour hopping amplitude $t_{pd\sigma}$, Δ_{cf} and Δ_{ct}, are shown in the inset of Fig. 5. As the 3*d* bandwidth arises mainly through Mn 3*d*–O 2*p* hybridization ($W \propto t_{pd}^2/\Delta_{ct}$), the increase of t_{pd} hopping with pressure is to some extent compensated by the overall lowering of the *p* bands (increase in Δ_{ct}).

So far we have demonstrated a connection between the moment collapse and metal–insulator transition, yet the chicken-and-egg question—which property drives? which property follows?—is not yet answered. To this end, we have carried out a further calculation at $v = 0.8$ (well within the insulating high-spin state) without any intra-atomic exchange ($J = 0$). In spite of the large U and same U/W ratio, a low-spin solution is obtained, which is metallic although strongly renormalized. This result clearly shows that the metal–insulator transition is driven by the collapse of the moment, which cannot withstand the increase of Δ_{cf}. The transition is characterized as evolving from five half-filled bands $t_{2g} + e_g$ (high spin) to three t_{2g} bands with one hole per site (low spin), as shown in Fig. 4. The interaction energy cost of moving an electron from site to site is determined by $U_{eff} = d^{n+1} + d^{n-1} - 2d^n$. Using the atomic configurations corresponding to high-spin and low-spin states, we arrive at an effective repulsion[32] $U_{eff}^{HS} = U + 4J = 10.3$ eV and $U_{eff}^{LS} = U - J = 5.9$ eV respectively, indicating much stronger inhibition of the electron propagation in the high-spin state. Moreover, the Mn $3d(e_g)$–O 2*p* hybridization provides a further screening channel for the effective t_{2g}–t_{2g} interaction in the low-spin state. Indeed, a calculation carried out in the low-spin state with O 2*p* states integrated out (keeping the 3*d* bandwidth unchanged) before solving the interacting problem leads to more pronounced

high-energy shoulders as compared with the solution with O $2p$ states fully included.

These results establish that the transition is controlled by competition between the crystal-field spitting Δ_{cf} (favouring the low-spin state) and the intra-atomic exchange coupling J (favouring the high-spin state). Although both energy scales are important for the outcome of the calculations, only the former (Δ_{cf}) is sensitive to an applied pressure. The importance of the value of J was also found in LDA + U studies of the Mott transition[26]. Recently, Werner and Millis[33] studied a two-band model with competing intra-atomic exchange and crystal-field splitting. In the parameter range relevant for the present study, they found three different phases realized in the following order with increasing crystal-field splitting: (1) spin-polarized Mott insulator, (2) metal with large orbital and spin fluctuations and (3) orbitally polarized insulator. Moreover, they found an orbitally selective closing of the gap on doping in the vicinity to the (1)–(2) phase boundary. The correspondence between their spin-polarized insulator phase (1) and the high-spin state of MnO is evident. The transition regions in MnO and phase (2) are both characterized by metallization and strong orbital fluctuations as well as the orbitally selective gap behaviour. In addition, the low-spin state of MnO and phase (3) of the model exhibit similarity, the orbital polarization. The insulating character of their phase (3) is dictated by band-filling and does not invalidate the above analogy.

Like almost all previous studies using LDA + DMFT, we have included only the density–density terms of the Coulomb repulsion. Although they are not expected to influence a first-order volume collapse (see the next section) especially above 1,000 K, it is gratifying to obtain some confirmation. Werner and Millis used the full Coulomb interaction in their study, and the similarity of the behaviour of their model to what is found here for MnO provides some verification of the unimportance of the neglected terms.

EQUATION OF STATE AND THE CRITICAL PRESSURE

To compare to high-pressure experiments, knowledge of phase stability is needed, which can be obtained from free energy versus volume (equation of state). The theoretical justification for applying DMFT using the underlying LDA description relies on a well-defined thermodynamic grand canonical potential functional, for which specific realizations have been suggested[15,27,34]. As it is difficult to extract the entropic term[28] in the free energy, we restrict ourselves to evaluation of the internal energy; in any case the variation of the entropy term is very small on the energy scale of several electronvolts involved in the changes of total energy, and the change in spin entropy will be partially compensated by a change in orbital entropy. We use the internal energy scheme of McMahan and co-workers[15,27,28] that is similar to that of Savrasov and Kotliar[34] corresponding to the expression $E(V,T) = E_{\mathrm{LDA}}(V) + [E_{\mathrm{DMFT}}(V,T) - E_{\mathrm{MF}}(V)]$, where E_{LDA} is the all-electron (unpolarized) LDA energy, E_{DMFT} is the internal energy corresponding to the self-consistent (dynamic) DMFT solution for the effective hamiltonian and E_{MF} is the static mean-field internal energy. The equation-of-state curve is shown in Fig. 5, both as $E(V)$ and converted to $V(P)$. The main feature is the deviation from convexity in the transition region, which leads to a calculated volume collapse $v^{\mathrm{th}} = 0.68 \rightarrow 0.59$ at $P_c^{\mathrm{th}} = 120$ GPa. The metallization and moment collapse obtained here are not far from the high-pressure data[8–10], with the transition volume (pressure) being smaller (larger) than the experimental values $v_c^{\mathrm{exp}} = 0.68 \rightarrow 0.63$, $P_c^{\mathrm{exp}} = 100$ GPa. The state just above the collapse is a high-spin insulator, with the t_{2g} gap about to close. The collapsed state is low spin, the e_g gap having just closed making it metallic in both subshells.

OUTLOOK

These results demonstrate that the underlying LDA band structure, buttressed by onsite interactions (U, J) treated within the dynamical DMFT ansatz, provides a realistic description of the Mott transition in MnO without input from experiment. This study finally enables determination of the mechanism of the transition, which could not be uncovered by experiment alone: the magnetic moment collapse, volume collapse and metal–insulator transitions occur simultaneously, but it is the increasing crystal-field splitting (encroachment of the O^{2-} ion on the internal structure of the Mn ion) and not the increasing bandwidth that tips the balance.

The current results illustrate success of the LDA + DMFT approach in describing a pressure-driven Mott transition in a strongly correlated insulator, joining the growing number of successes of this approach in other strongly correlated real materials. The Kondo volume collapse transition in Ce (refs 15,28) and other elemental lanthanides[27] and the realistic modelling of parts of the complex phase diagram[16] and multiplet effects[35] in Pu reflect the progress in correlated metals, with low-temperature properties (heavy fermion characteristics) remaining an imposing challenge. Impressive progress has also been demonstrated in the description of structurally driven[17,36] and doping-driven[37] metal–insulator transitions in transition-metal oxides. Excitation spectra[21,22] of the charge-transfer compound NiO at ambient pressure, where O $2p$ states are entangled with the $3d$ states, have shown excellent agreement with experiment. These results on MnO bring a further class of materials into the list of strongly correlated systems whose behaviour is becoming understood owing to recent theoretical developments.

METHODS

SINGLE-PARTICLE HAMILTONIAN AND INTERACTION TERM

The LDA + DMFT computational scheme[19] in its present implementation, applied previously to NiO (refs 21,22), proceeds in two steps: (1) construction of an effective multi-band Hubbard hamiltonian H via Wannier transformation from a converged (unpolarized, metallic) LDA solution corrected for double counting of the onsite interaction, and (2) self-consistent solution of the DMFT equations[12,20] using the quantum Monte Carlo (QMC) impurity solver[38].

$$
\begin{aligned}
H = & \sum_{\mathbf{k},\sigma,\alpha,\beta} h^{dd}_{\mathbf{k},\alpha\beta} d^{\dagger}_{\mathbf{k}\alpha\sigma} d_{\mathbf{k}\beta\sigma} + \sum_{\mathbf{k},\sigma,\gamma,\delta} h^{pp}_{\mathbf{k},\gamma\delta} p^{\dagger}_{\mathbf{k}\gamma\sigma} p_{\mathbf{k}\delta\sigma} \\
& + \sum_{\mathbf{k},\sigma,\alpha,\gamma} h^{dp}_{\mathbf{k},\alpha\gamma} d^{\dagger}_{\mathbf{k}\alpha\sigma} p_{\mathbf{k}\gamma\sigma} + \sum_{\mathbf{k},\sigma,\gamma,\alpha} h^{pd}_{\mathbf{k},\gamma\alpha} p^{\dagger}_{\mathbf{k}\gamma\sigma} d_{\mathbf{k}\alpha\sigma} \\
& + \sum_{i,\sigma,\sigma',\alpha,\beta} \mathcal{U}^{\sigma\sigma'}_{\alpha\beta} n^{d}_{i\alpha\sigma} n^{d}_{i\beta\sigma'},
\end{aligned}
$$

where $d_{\mathbf{k}\alpha\sigma}$ ($p_{\mathbf{k}\gamma\sigma}$) is the Fourier transform of the operator $d_{i\alpha\sigma}$ ($p_{i\gamma\sigma}$), which annihilates the d (p) electron with orbital and spin indices $\alpha\sigma$ ($\gamma\sigma$) in the ith unit cell, and $n^{d}_{i\alpha\sigma}$ is the corresponding d occupation number operator.

The single-particle part of the hamiltonian was obtained by a Wannier function projection method[39], which amounts to a unitary transformation in the Hilbert space containing Mn $3d$, O $2p$ bands and the next-lowest empty (polarization) conduction band. The site energy of the Mn $3d$ orbitals was corrected for double counting of the d–d interaction by subtracting from the LDA site energy ε_d a Hartree-like term giving $\varepsilon_d^{\circ} = \varepsilon_d - (N-1)\bar{U} n_{\mathrm{LDA}}$, where $N = 10$ is the total number of orbitals per Mn site, $\bar{U}$ is the average Coulomb repulsion and n_{LDA} is the average occupancy per d orbital. As the p–d band separation Δ_{ct} in MnO, which is to some extent influenced by the choice of the double-counting term, is large in the transition region, small variation of Δ_{ct} will not change the results.

THE COULOMB INTERACTION MATRIX

The onsite Coulomb interaction $\mathcal{U}^{\sigma\sigma'}_{\alpha\beta}(U,J)$ within the Mn $3d$ shell, restricted to only density–density terms, was expressed as usual[40] in terms of the direct

(U) and exchange (J) interaction strengths related to the Slater integrals F_0, F_2, F_4. The numerical values[32] of $U = 6.9$ eV and $J = 0.86$ eV were obtained by the constrained LDA method[41]. As they exhibit only a small pressure dependence, these values were used for all volumes. We used $L = 100$ imaginary time points in the Monte Carlo simulation, in which the standard single-field-flip moves were augmented by special global moves that played a crucial role in ensuring ergodic sampling in the transition region. To obtain an indication of the robustness of our results we carry out, in parallel with these *ab initio* interaction strengths, calculations with an enhanced (by 15%) value of $J = 1$ eV (and fixed U/J ratio). All of the presented results were obtained at the temperature $T = 1{,}160$ K, in the rock-salt structure.

MONTE CARLO PROCEDURE; INTRODUCTION OF GLOBAL MOVES

The DMFT equations were solved numerically on a Matsubara contour (using asymptotic expansions for frequencies $\omega_n > 500$ eV), and the k-space integrals were carried out by summation over 3,375 k-points in the first Brillouin zone. The chemical potential was adjusted in each DMFT iteration to guarantee the total electron count of 11 ± 10^{-6}. The impurity problem was solved using the Hirsch–Fye QMC algorithm[38] modified for multiple orbitals. The onsite interaction was decoupled using a single binary Hubbard–Stratonovich auxiliary field $S_{\alpha\beta}(l)$ for each pair of orbitals $\alpha\beta$ and each of L imaginary time slices (45 auxiliary fields for each time slice).

The key innovation in this application to MnO in the transition regime was introduction of global Monte Carlo moves in addition to the usual single flips of the auxiliary fields. These moves allow for fluctuations between high-spin- and low-spin-like configurations, which are otherwise practically unreachable with the standard single-auxiliary-field-flip moves. The purpose of global moves is to mimic transferring electrons between orbitals. In general there is no straightforward relationship between a given configuration of auxiliary fields, described by a binary L-vector $S_{\alpha\beta}$ and the occupancy of orbitals. However, in the case of two atomic orbitals, the probability distribution is peaked around auxiliary field configurations corresponding to a particular orbital occupancy, and flipping all fields corresponds to swapping occupancies of the two orbitals[42]. This can be generalized to multiple orbitals as follows. To swap occupancies of orbitals α and β, we have to: (1) flip fields in $S_{\alpha\beta}$, (2) for all remaining fields in orbitals γ coupled to orbitals α or β swap the configurations $S_{\gamma\alpha} \leftrightarrow S_{\gamma\beta}$. As the decoupling is antisymmetric with respect to the ordering of orbitals, auxiliary fields must be flipped in step (2) whenever the order of orbitals changes between $S_{\gamma\alpha}$ and $S_{\gamma\beta}$.

Testing several types of the above moves, we found that only simultaneous moves of two electrons between t_{2g} and e_g orbitals of opposite spin (that is, moves intuitively expected in low-spin $\leftrightarrow$ high-spin fluctuations) have appreciable acceptance. The acceptance rate of the global moves was found to be large only in the transition regime, which had been characterized by unusually slow convergence of the DMFT cycle. We checked for the possibility of multiple solutions, but found none at the temperature of these simulations. The numerical value of the total energy, limited by the stochastic error of the E_{DMFT} term, was converged to the accuracy of 0.06 eV in the transition regime and 0.02 eV anywhere else. The spectral densities were calculated by the maximum entropy analytic continuation technique[43] applied to the imaginary-time Green functions from 4×10^7–6×10^7 QMC-simulation sweeps collected into 2,000–20,000 bins.

Received 27 July 2007; accepted 7 January 2008; published 3 February 2008.

References

1. Mott, N. F. The Basis of the electron theory of metals, with special reference to the transition metals. *Proc. Phys. Soc. Lond. A* **62**, 416–422 (1949).
2. Mott, N. F. Metal–insulator transition. *Rev. Mod. Phys.* **40**, 677–683 (1968).
3. Imada, M., Fujimori, A. & Tokura, Y. Metal–insulator transitions. *Rev. Mod. Phys.* **70**, 1039–1263 (1998).
4. Saitoh, T., Bouquet, A. E., Mizokawa, T. & Fujimori, A. Systematic variation of the electronic structure of 3d transition-metal compounds. *Phys. Rev. B* **52**, 7934–7938 (1995).
5. Noguchi, Y., Kusaba, K., Fukuoka, K. & Syono, Y. Shock-induced phase transition of MnO around 90 GPa. *Geophys. Res. Lett.* **23**, 1469–1472 (1996).
6. Mita, Y. *et al.* Optical study of MnO under pressure. *Phys. Status Solidi B* **223**, 247–251 (2001).
7. Mita, Y., Izaki, D., Kobayashi, M. & Endo, S. Pressure-induced metallization of MnO. *Phys. Rev. B* **71**, 100101 (2005).
8. Patterson, J. R. *et al.* Pressure-induced metallization of the Mott insulator MnO. *Phys. Rev. B* **69**, 220101 (2004).
9. Yoo, C. S. *et al.* First-order isostructural Mott transition in highly compressed MnO. *Phys. Rev. Lett.* **94**, 115502 (2005).
10. Rueff, J.-P., Mattila, A., Badro, J., Vankò, G. & Shukla, A. Electronic properties of transition-metal oxides under high pressure revealed by X-ray emission spectroscopy. *J. Phys. Condens. Matter* **17**, S717–S726 (2005).
11. Metzner, W. & Vollhardt, D. Correlated lattice fermions in $d = \infty$ dimensions. *Phys. Rev. Lett.* **62**, 324–327 (1989).
12. Georges, A., Kotliar, G., Krauth, W. & Rozenberg, M. J. Dynamical mean-field theory of strongly correlated fermion systems and the limit of infinite dimensions. *Rev. Mod. Phys.* **68**, 13–125 (1996).
13. Kotliar, G. & Vollhardt, D. Strongly correlated materials: Insights from dynamical mean-field theory. *Phys. Today* **57**, 53–59 (2004).
14. Lichtenstein, A. I. & Katsnelson, M. I. Ab initio calculations of quasiparticle band structure in correlated systems: LDA++ approach. *Phys. Rev. B* **57**, 6884–6895 (1998).
15. Held, K., McMahan, A. K. & Scalettar, R. T. Cerium volume collapse: Results from the merger of dynamical mean-field theory and local density approximation. *Phys. Rev. Lett.* **87**, 276404 (2001).
16. Savrasov, S., Kotliar, G. & Abrahams, E. Electronic correlations in metallic plutonium within dynamical mean-field picture. *Nature* **410**, 793–795 (2001).
17. Held, K., Keller, G., Eyert, V., Vollhardt, D. & Anisimov, V. I. Mott-Hubbard metal–insulator transition in paramagnetic V_2O_3: An LDA + DMFT(QMC) study. *Phys. Rev. Lett.* **86**, 5345–5348 (2001).
18. Georges, A. Strongly correlated electron materials: Dynamical mean field theory and electronic structure. *AIP Conf. Proc.* **715**, 3–73 (2004).
19. Held, K. *et al.* Realistic investigations of correlated electron systems with LDA + DMFT. *Phys. Status Solidi B* **243**, 2599–2631 (2006).
20. Kotliar, G. *et al.* Electronic structure calculations with dynamical mean field theory. *Rev. Mod. Phys.* **78**, 865–951 (2006).
21. Kuneš, J., Anisimov, V. I., Lukoyanov, A. V. & Vollhardt, D. Local correlations and hole doping in NiO: A dynamical mean field study. *Phys. Rev. B* **75**, 165115 (2007).
22. Kuneš, J., Anisimov, V. I., Skornyakov, S. L., Lukoyanov, A. V. & Vollhardt, D. NiO: Correlated band structure of a charge-transfer insulator. *Phys. Rev. Lett.* **99**, 156404 (1997).
23. Cohen, R. E., Mazin, I. I. & Isaak, D. G. Magnetic collapse in transition metal oxides at high pressure: Implications for the Earth. *Science* **275**, 654–657 (1997).
24. Fang, Z., Solovyev, I. V., Sawada, H. & Terakura, K. First principles study on electronic structures and phase stability of MnO and FeO under high pressure. *Phys. Rev. B* **59**, 762–774 (1999).
25. Kasinathan, D. *et al.* Mott transition of MnO under pressure: comparison of correlated band theories. *Phys. Rev. B* **74**, 195110 (2006).
26. Kasinathan, D., Koepernik, K. & Pickett, W. E. Pressure-driven magnetic moment collapse in the ground state of MnO. *New J. Phys.* **9**, 235–246 (2007).
27. McMahan, A. K., Held, K. & Scalettar, R. T. Thermodynamic and spectral properties of compressed Ce calculated using a combined local-density approximation and dynamical mean field theory. *Phys. Rev. B* **67**, 075108 (2003).
28. McMahan, A. K. Combined local-density and dynamical mean field theory calculations for the compressed lanthanides Ce, Pr, and Nd. *Phys. Rev. B* **72**, 115125 (2005).
29. van Elp, J., Potze, R. H., Eskes, H., Berger, R. & Sawatzky, G. A. Electronic structure of MnO. *Phys. Rev. B* **44**, 1530–1537 (1991).
30. Liebsch, A. Mott transitions in multiorbital systems. *Phys. Rev. Lett.* **91**, 226401 (2003).
31. Koga, A., Kawakami, N., Rice, T. M. & Sigrist, M. Orbital-selective Mott transitions in the degenerate Hubbard model. *Phys. Rev. Lett.* **92**, 216402 (2004).
32. Anisimov, V. I., Zaanen, J. & Andersen, O. K. Band theory and Mott insulators: Hubbard U instead of Stoner I. *Phys. Rev. B* **44**, 943–954 (1991).
33. Werner, P. & Millis, A. J. High-spin to low-spin and orbital polarization transitions in multiorbital Mott systems. *Phys. Rev. Lett.* **99**, 126405 (2007).
34. Savrasov, S. Y. & Kotliar, G. Spectral density functionals for electronic structure calculations. *Phys. Rev. B* **69**, 245101 (2004).
35. Shick, A., Havela, L., Kolorenc, J. & Drchal, V. Multiplet effects in the electronic structure of δ-Pu, Am and their compounds. *Europhys. Lett.* **77**, 17003 (2007).
36. Pavarini, E. *et al.* Mott transition and suppression of orbital fluctuations in orthorhombic $3d^1$ perovskites. *Phys. Rev. Lett.* **92**, 176403 (2004).
37. Craco, L., Laad, M. S., Leoni, S. & Muller-Hartmann, E. Insulator–metal transition in the doped $3d^1$ transition metal oxide $LaTiO_3$. *Phys. Rev. B* **70**, 195116 (2004).
38. Hirsch, J. E. & Fye, R. M. Monte Carlo method for magnetic impurities in metals. *Phys. Rev. Lett.* **56**, 2521–2524 (1986).
39. Anisimov, V. I. *et al.* Full orbital calculation scheme for materials with strongly correlated electrons. *Phys. Rev. B* **71**, 125119 (2005).
40. Shick, A. B, Liechtenstein, A. I. & Pickett, W. E. Implementation of the LDA + U method using the full potential linearized augmented plane wave basis. *Phys. Rev. B* **60**, 10763–10769 (1999).
41. Anisimov, V. I. & Gunnarsson, O. Density functional calculation of effective Coulomb interactions in metals. *Phys. Rev. B* **43**, 7570–7574 (1991).
42. Scalettar, R. T., Noack, R. M. & Singh, R. R. P. Ergodicity at large couplings with the determinant Monte Carlo algorithm. *Phys. Rev. B* **44**, 10502–10507 (1991).
43. Jarrell, M. & Gubernatis, J. E. Bayesian inference and the analytic continuation of imaginary-time quantum Monte Carlo data. *Phys. Rep.* **269**, 133–195 (1996).

Acknowledgements

J.K. gratefully acknowledges the Research Fellowship of the Alexander von Humboldt Foundation. We acknowledge numerous discussions with D. Vollhardt and A. K. McMahan, and useful interaction with K.-W. Lee during the latter stages of this work. This work was supported by SFB 484 of the Deutsche Forschungsgemeinschaft (J.K.), by the Russian Foundation for Basic Research under the grants RFFI-06-02-81017, RFFI-07-02-00041 (V.I.A. and A.V.L.) and the Dynasty Foundation (A.V.L.), by DOE grant No. DE-FG02-04ER46111 and by DOE Strategic Science Academic Alliance grant No. DE-FG01-06NA26204. This research was also encouraged and supported by the US Department of Energy's Computational Materials Science Network (J.K., R.T.S. and W.E.P.).
Correspondence and requests for materials should be addressed to J.K.
Supplementary Information accompanies this paper on www.nature.com/naturematerials.

Author contributions

J.K. wrote the code and performed the DMFT (QMC) calculations. J.K., R.T.S., W.E.P. and V.I.A. formulated the approach and chose the application to MnO. A.V.L. and V.I.A. calculated the LDA quantities and carried out the Wannier transformation to the local representation. J.K. and W.E.P. wrote the paper.